

Source Parameters of Regional Earthquakes in Taiwan: July 1995–December 1996

Honn Kao¹ and Pei-Ru Jian¹

(Manuscript received 24 March 1998, in final form 28 May 1999)

ABSTRACT

Systematic determination of reliable source parameters for regional earthquakes in Taiwan, particularly offshore events with $m_b < 5.5$, has been a difficult task because of poor coverage by the local network and the lack of signals at teleseismic distances. Establishment of the “Broadband Array in Taiwan for Seismology (BATS)” has greatly improved such a task through moment-tensor inversion of regional waveforms. Our inversion algorithm differs from previous studies in two major aspects. First, we evaluate the characteristics of background noise for individual stations. The results are then used to determine the lower corner of the frequency band used in the inversion to maximize the long-period information in waveforms. The higher corner is set at 0.06–0.08 Hz to avoid the effects of strong lateral heterogeneity and possible epicentral mislocation. Second, to further reduce the uncertainty caused by complex structures, a two-step procedure is adapted to select the best velocity models for different stations in calculating the synthetics. The inversion quality is classified by a combination of a letter (A–F) and a digit (1–4) reflecting the waveform misfit and the compensated linear vector dipole (CLVD) component, respectively. In total, source parameters of 36 events that occurred between July 1995 and December 1996 are reported in this study. For the few events that are big enough to be studied teleseismically, most of our solutions are consistent with those reported by other institutions. We intend to make our inversion results available on a routine basis that they will not only be able to provide precise source parameters for smaller regional earthquakes, but will also serve as an alternative to independently examine solutions of large and moderate-sized events reported from other sources.

(Key words: Broadband seismic network, Earthquake source parameter, Waveform inversion, Taiwan)

1. INTRODUCTION

Precise determination of seismic source parameters is a fundamental issue in earthquake

¹Institute of Earth Sciences, Academia Sinica, Taipei, Taiwan, ROC

studies. Since the early 80's, both the development of centroid-moment-tensor (CMT) inversion technique and increasing coverage of global digital seismic networks have led to the success of systematic determination of earthquake source parameters in large quantity (e.g., Dziewonski et al., 1981; Kawakatsu et al., 1995; Sipkin, 1982). Unfortunately, the CMT catalogs cover only large and moderate-sized events that generate sufficient signals at teleseismic distances.

Recently, with increasing knowledge of detailed velocity structures on a regional scale and the establishment of regional broadband networks, extracting CMT solutions from regional waveforms has become feasible (e.g., Dreger and Helmberger, 1993; Fan and Wallace, 1995; Lay et al., 1994; Thio and Kanamori, 1995; Zhao and Helmberger, 1994). In fact, point-source CMT inversion has become routine practice for regional earthquakes occurring in the western U.S. (e.g., Zhu and Helmberger, 1996; Pasynos et al., 1996).

In mid-1992, the Institute of Earth Sciences (IES), Academia Sinica, along with several domestic and foreign institutions, began to prepare a prospectus for establishing a broadband seismic network in the Taiwan region. The network, named "Broadband Array in Taiwan for Seismology (BATS)," is designed with 15 permanent stations located on Taiwan and the surrounding islands with additional 15 portable units (Figure 1). The test operation began in late 1994.

One of BATS' original goals is to routinely estimate source parameters of earthquakes occurring in the region, particular those offshore events east of Taiwan where coverage by the local network is poor. The stability and tectonic implications of our work have been demonstrated in a previous study (Kao et al., 1998a). The purpose of this paper is to systematically present source parameters of regional events with which we were able to perform moment-tensor inversion using BATS data. Earthquakes that occurred between July 1995 and December 1996 are included in this report and we intend to make the results for events after December 1996 available on a routine basis. Our results not only provide precise source parameters for smaller regional events that cannot be determined otherwise, but also serve as an alternative to independently examine solutions of large and moderate-sized events from other sources.

2. BATS DATA AND ANALYSIS

The BATS instrumentation is designed to cover a variety of research demands. All permanent stations are equipped with state-of-the-art very-broadband (Streckeisen STS-1 or STS-2) and strong-motion (Terra Technology SSA-320) sensors and 24-bits digital recorders (Quanterra Q-680 or Q-4120). Data streams with high sampling rates (≥ 80 samples per s) are recorded in triggering mode, while others are recorded in continuous mode on both hard disks and magnetic tapes. All stations are capable of telecommunication for immediate retrieval of specific events. Preliminary data quality control is performed at IES. Afterwards, the data are contributed to the Data Management Center of the Incorporated Research Institutions for Seismology (DMC, IRIS) for distribution.

Distinct from many previous studies, our analysis begins with a background-noise evaluation that determines the frequency band used in the inversion. Cut-off frequency of the lower

Broadband Array in Taiwan for Seismology

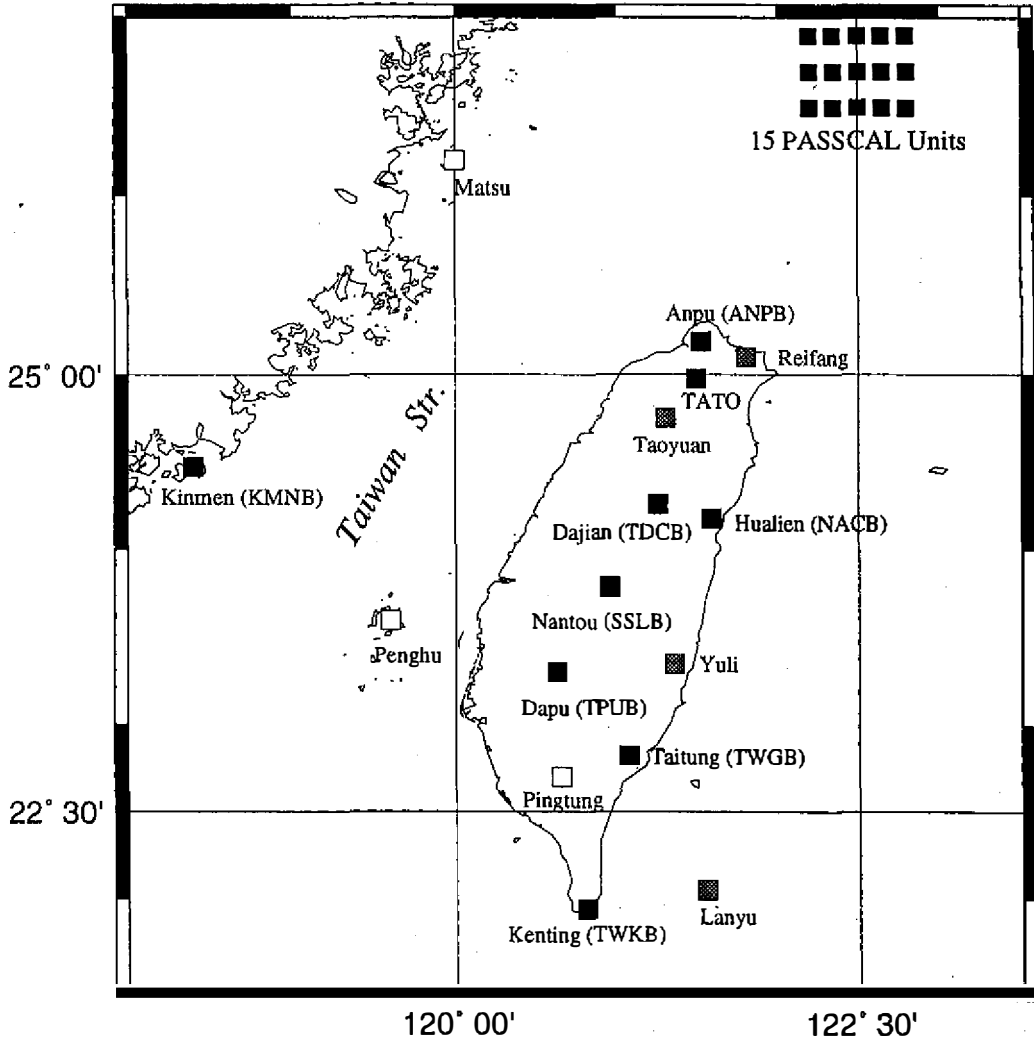


Fig. 1. Map of the “Broadband Array in Taiwan for Seismology (BATS).” Solid and grey squares show stations currently in operation and under construction, respectively, while the open squares represent stations planned for the near future. In addition to the permanent stations, BATS includes 15 portable stations that can be deployed for specific research tasks (as represented by symbols near the upper-right corner).

corner is determined by comparing the power spectra of waveform windows 300 s before and after the *P* first arrival (Figure 2). It is set at the frequency where the signal-to-noise (S/N) ratio increases to at least 2.0 which, based on our experiences, is usually at ~0.02 Hz (Figure 2). The higher corner, on the other hand, is set at 0.06–0.08 Hz to avoid the effect of lateral heterogeneity and to simplify the calculation of synthetics. The waveform is discarded if the bandwidth between the two corners is too narrow to warrant a reliable inversion.

The velocity model used to generate synthetic seismograms is adapted from the average 1-D model proposed by Rau and Wu (1995). The original model consists of 12 layers, but we found that a simplified one with three layers representing the upper crust, the lower crust, and the mantle half-space, respectively, is sufficient to reproduce the waveform's long-period characteristics, as shown in Figure 3. Consequently, we adapt the three-layer simplified velocity model in this study to reduce the computation load.

Although long-period waveforms are not sensitive to crustal details, certain knowledge on the approximate crustal thickness turns out to be necessary in deriving the correct Green's functions. To further minimize the uncertainty caused by incorrect Moho depth, we utilize a two-step procedure to allow different velocity models for different stations. The selection begins with a joint inversion of all available data using a common 1-D model. Then we fix the derived focal mechanism and adjust the velocity model for each station in a forward sense. Currently, we have set up 7 different velocity models with Moho depths ranging from 15 to 45 km.

Our inversion algorithm is based on the linear relationship between waveforms and the six elements of a moment tensor (Aki and Richards, 1980). Computation of the Green's functions is done with the computational technique from Yao and Harkrider (1983) that efficiently combines the reflectivity method (Kennett, 1980) and the discrete wavenumber summation method (Bouchon, 1981). The calculation time for Green's functions is on the order of 10 minutes, while the inversion itself usually takes no more than 30 s. In practice, we stored all the calculated Green's functions online to accelerate the overall performance (Dreger and Helmberger, 1993).

All waveforms are normalized to a distance of 100 km to eliminate the amplitude bias caused by geometric spreading and attenuation. Different weightings are assigned in the inversion according to the quality of waveforms. Finally, all synthetics are allowed to shift in time with respect to observations such that the corresponding cross-correlation reaches the maximum. The tolerable time shift is set at ± 3 s.

We evaluate the goodness of the inversion by three parameters. The first is the amount of isotropic component, defined as

$$\phi = (\sum m_i / 3) \times (1 / |m|_{\max}) \quad (1)$$

where $\sum m_i$ is the sum of the three eigenvalues of the moment tensor and $|m|_{\max}$ is the largest absolute value. A ϕ of 1, -1, and 0 corresponds to an explosion, implosion, and zero-volume change, respectively. For most cases, the inversion gives a $|\phi| < 0.1$. In the case of a larger ϕ , a *a priori* constraint of $\phi \sim 0$ is imposed to stabilize the inversion process.

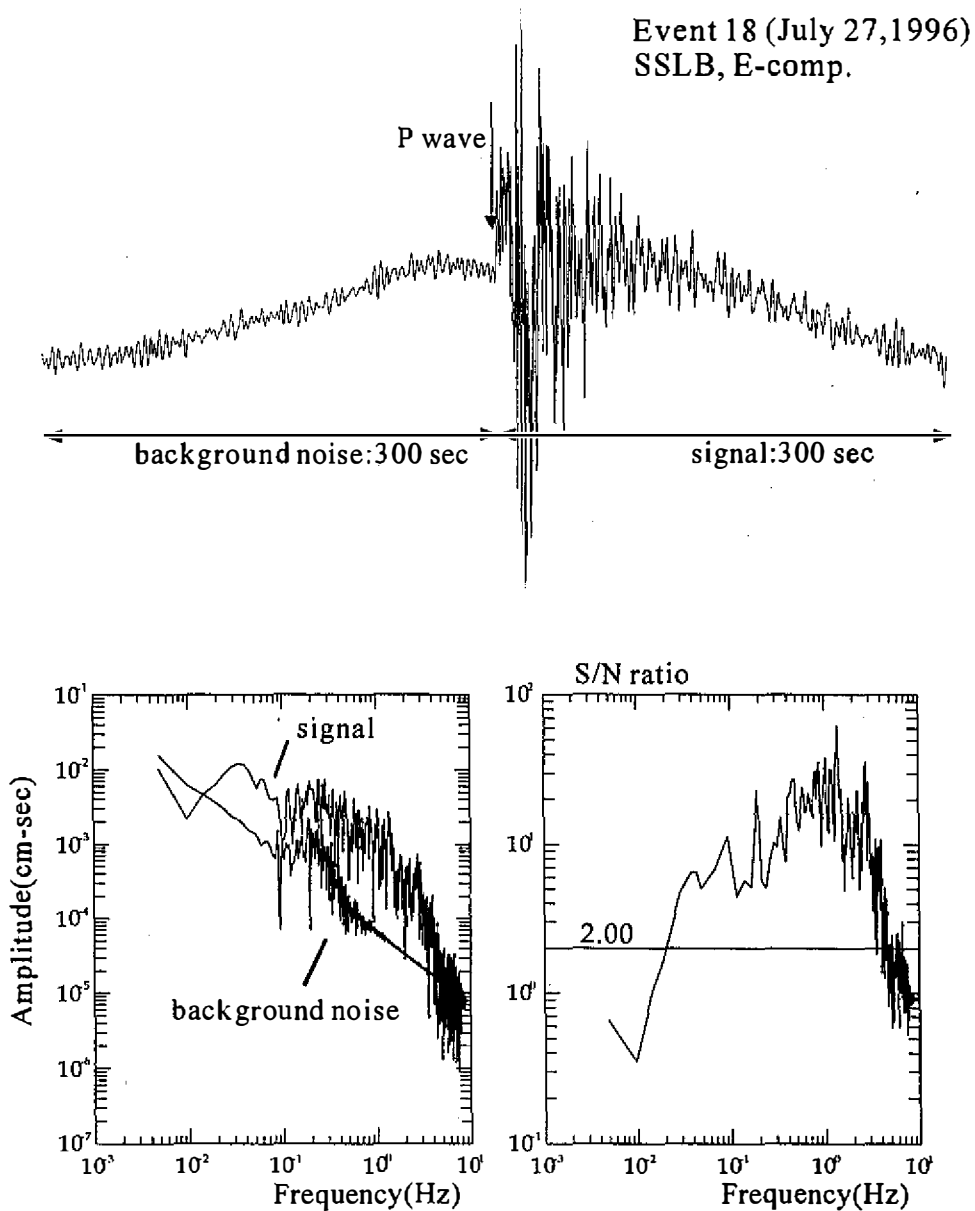


Fig. 2. Example showing the determination of the lower corner of the frequency band used in the inversion. The upper panel shows the original seismogram and the two time windows, background noise and signal, defined as 300 s before and after the *P* arrival, respectively. The lower panel shows the corresponding frequency spectra (left) and the signal-to-noise (S/N) ratio with respect to frequency (right). It is set at the frequency where the S/N ratio increases to at least 2.0.

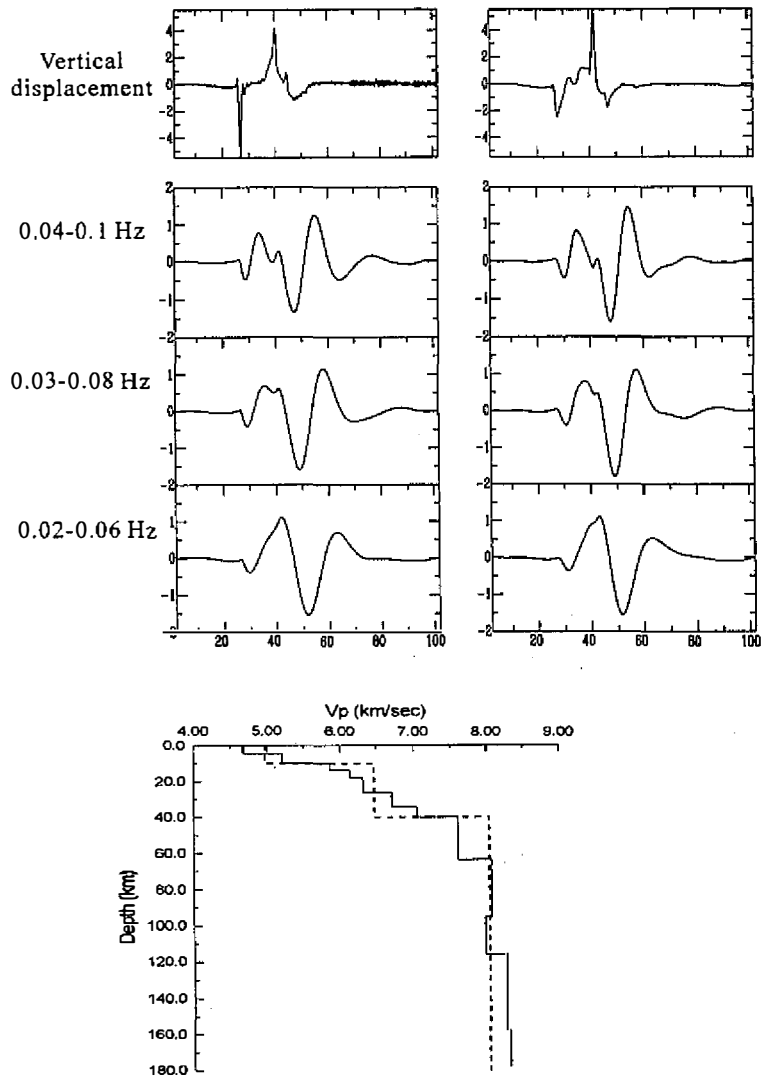


Fig. 3. Synthetic seismograms to demonstrate the insensitivity of long-period waveforms to velocity structural detail. The left traces in the top panel are ground displacements generated with the average 1-D model proposed by Rau and Wu (1995) (solid line in the lower panel), whereas the right traces are associated with a simplified model consisting of only 3 layers (dashed line in the lower panel). It is clear that for the frequency band used in this study, the waveform difference between the two velocity models is insignificant. Source is assumed to be a vertical dip slip fault. Epicentral azimuth and distance are 120° and 207 km, respectively.

The second parameter is to measure the deviation from a pure double-couple source (Dziewonski et al., 1981),

$$\varepsilon = 2 \times (|m^*|_{\min} / |m^*|_{\max}) \quad (2)$$

where $m^* = m - (\Sigma m_i / 3)$. ε is 0 and 1 for a pure double couple and a CLVD source, respectively.

The third is the misfit between the observed and synthetic waveforms. In our previous study (Kao et al., 1998a), the misfit was defined as

$$E = 1 - \{ \int f g dt / [(\int f^2 dt)^{1/2} (\int g^2 dt)^{1/2}] \} \quad (3)$$

where f and g are observed and synthetic seismograms, respectively (Mellman et al., 1975). It is 0 if there is a perfect fit. The advantage of this formula is that it is relatively more sensitive to the correlation of waveforms rather than the absolute amplitudes (Wallace et al., 1981). Thus, knowing *a priori* structural details becomes less critical. On the other hand, ignorance of the absolute amplitudes might cause the inversion to be less stable, making it necessary to include waveforms recorded at various azimuths.

In this study, we choose a slightly modified formula to measure the misfit, defined as

$$E = 1 - (f_{\max} / g_{\max}) \times \{ \int f g dt / [(\int f^2 dt)^{1/2} (\int g^2 dt)^{1/2}] \} \quad (4)$$

where f_{\max} and g_{\max} are the maximum amplitudes measured from observed and synthetic seismograms, respectively (Zeng and Anderson, 1996). This formula is an excellent compromise between formula (3) that considers only the correlation between waveforms and the conventional root-mean-square (RMS) error that is determined completely by the amplitude differences. The quality of inversion is classified by a combination of a letter (A–F) and a digit (1–4). These are dictated by the waveform misfit (E) and the amount of CLVD component (ε), respectively, and are listed in Table 1.

3. INVERSION RESULTS

We have applied the above technique to estimate source parameters of regional events with $M_L \geq 4.5$ in Taiwan. Because of various problems in the early stage of BATS, including an insufficient number of stations, unexpected power and instrument failure, and high background noise level, the inversion gives low-quality or even no solutions for many events in 1995 and 1996. In this paper, we report source parameters only if they meet the following criteria: (1) 3-component waveforms from at least three stations are used in the inversion, and (2) the quality of inversion must be higher than C4. In total, inversion results for 36 earthquakes satisfy these conditions and are listed in Table 2. The best double solutions and focal depths are also plotted in Figure 4.

Table 1. Quality classification of inversion results.

| Class | Criteria |
|-------------------------------|----------------------------|
| Average Waveform Misfit (E) | |
| A | $0 \leq E < 0.3$ |
| B | $0.3 < E \leq 0.5$ |
| C | $0.5 < E \leq 0.7$ |
| D | $0.7 < E \leq 0.9$ |
| E | $0.9 < E \leq 1.1$ |
| F | $E > 1.1$ |
| CLVD component (ϵ) | |
| 1 | $\epsilon \leq 0.1$ |
| 2 | $0.1 < \epsilon \leq 0.25$ |
| 3 | $0.25 < \epsilon \leq 0.4$ |
| 4 | $\epsilon > 0.4$ |

Due to the limited space, we show three representative examples in this section. The first is an offshore event that occurred in the southernmost segment of the Ryukyu subduction zone to the NE of Taiwan (No. 18, Table 2 and Figures 4 and 5). The second (No. 29, Table 2 and Figures 4 and 6) took place near the eastern coast of Taiwan, while the third (No. 6, Table 2 and Figures 4 and 7) is an inland event beneath the Coastal Plain in SW Taiwan. The complete inversion results are presented in the appendix and can be retrieved electronically from IES' anonymous ftp server (140.109.80.2 in /pub/BATS/mt_inv).

Eighteen observed waveforms (3 components at 6 stations) were used in the inversion of event No. 18. Evaluation of the background noise level indicated that the usable frequency bands were 0.03–0.08 Hz for TDCB and 0.02–0.06 Hz for the other stations (Figure 5). The best fitting result corresponds to a depth of 63 km, although there seems to be no significant difference among solutions from 60 to 66 km. Our inversion result indicates the orientation of *T*/*P*-axes along the subducted slab's downdip and the trench's strike directions, respectively. Such a pattern is consistent with the downdip extension at the depths between 70 and 150 km and the lateral compressive strain resulting from the regional collision, as reported in previous studies (Kao and Chen, 1991; Kao et al., 1998b). When overlapped with the available *P* first-motions recorded by the short-period network in Taiwan (circles and crosses in Figure 5), our solution can explain nearly all the reported onsets. Furthermore, our solution is fairly consistent with the CMT solution reported by Harvard University.

The second event (No. 29) is too small for teleseismic CMT inversion and the one-sided coverage by local stations makes the first motion solutions highly ambiguous (Figure 6). Our result shows a pure thrust mechanism with the *P*-axis in a NW–SE direction, which is consistent with the overall tectonic setting of collision in the region. Such a solution can also explain most of the reported *P* first motions (Figure 6). The inversion utilizes waveforms from 7 stations providing tight constraints on the focal depth at 18 ± 2 km.

Table 2. Source parameters of studied earthquakes.

| No. | O.T. ¹ | Lat. ¹ | Long. ¹ | Depth | M_{xx}^2 | M_{yy}^2 | M_{zz}^2 | M_{xy}^2 | M_{yz}^2 | M_{xz}^2 | M_w^2 | Str. ³ | Dip ³ | Rake ³ | ϵ^4 | ϵ^4 | Class |
|-----|---------------------|-------------------|--------------------|-------|------------|------------|------------|------------|------------|------------|---------|-------------------|------------------|-------------------|--------------|--------------|-------|
| 1 | 95/07/05/17:53:48.6 | 24.83 | 122.12 | 27 | -2.37 | 14.02 | -9.54 | -16.84 | 13.58 | -1.93 | 4.87 | 354 | 49 | -157 | 0.541 | 22.1 | C2 |
| 2 | 95/08/15/14:53:56.7 | 23.98 | 122.43 | 18 | -1.79 | -4.87 | 8.62 | 2.87 | 0.80 | 3.47 | 4.55 | 43 | 37 | 112 | 0.540 | 29.1 | C3 |
| 3 | 95/08/23/20:36:25.1 | 24.36 | 122.87 | 24 | -1.64 | 0.11 | 1.16 | 0.65 | 0.01 | -0.68 | 4.09 | 277 | 47 | 130 | 0.672 | 12.7 | C2 |
| 4 | 95/09/04/20:27:28.0 | 24.15 | 121.74 | 24 | -0.92 | -0.77 | 2.12 | 0.95 | -0.47 | -0.12 | 4.14 | 36 | 42 | 74 | 0.628 | 10.9 | C2 |
| 5 | 95/10/04/05:01:48.0 | 24.87 | 122.00 | 24 | 0.35 | 1.95 | -3.13 | -4.46 | 2.31 | 1.77 | 4.45 | 4 | 60 | -147 | 0.648 | 2.4 | C1 |
| 6 | 95/10/31/22:27:06.9 | 23.29 | 120.36 | 15 | -0.34 | -6.00 | 5.16 | 2.17 | 3.43 | -0.64 | 4.50 | 176 | 42 | 52 | 0.535 | 16.8 | C2 |
| 7 | 95/11/10/21:07:51.6 | 22.82 | 121.38 | 12 | 8.33 | -9.84 | 0.82 | 5.53 | -4.77 | -0.65 | 4.65 | 333 | 71 | 15 | 0.649 | 15.8 | C2 |
| 8 | 96/03/19/07:25:02.7 | 23.91 | 122.31 | 24 | -14.77 | 7.95 | 10.49 | -8.37 | 20.44 | -5.26 | 4.89 | 325 | 30 | 154 | 0.654 | 22.6 | C2 |
| 9 | 96/03/19/07:33:26.6 | 23.92 | 122.25 | 33 | -24.02 | 20.38 | 2.47 | -14.59 | 22.28 | -18.64 | 5.00 | 327 | 44 | 174 | 0.652 | 25.1 | C3 |
| 10 | 96/03/28/17:53:19.2 | 24.02 | 122.29 | 27 | -19.33 | 10.20 | 11.11 | -2.83 | 16.50 | -7.82 | 4.87 | 312 | 33 | 151 | 0.594 | 32.1 | C2 |
| 11 | 96/03/29/03:28:53.5 | 23.97 | 122.33 | 24 | -305.90 | 103.30 | 233.65 | 2.53 | 127.00 | -76.65 | 5.61 | 292 | 37 | 126 | 0.583 | 37.3 | C3 |
| 12 | 96/04/10/14:14:49.6 | 22.97 | 121.51 | 24 | 0.14 | -1.67 | 1.26 | 0.73 | -0.96 | 0.96 | 4.16 | 356 | 30 | 52 | 0.344 | 25.9 | B3 |
| 13 | 96/05/05/16:21:27.4 | 23.96 | 122.36 | 27 | -4.52 | 2.06 | 2.91 | -1.73 | 2.47 | -1.82 | 4.38 | 319 | 48 | 153 | 0.544 | 29.5 | C3 |
| 14 | 96/05/28/21:53:22.4 | 24.05 | 121.58 | 24 | -4.90 | -0.50 | 6.81 | 12.27 | 0.04 | 7.42 | 4.73 | 90 | 53 | 158 | 0.544 | 31.8 | C3 |
| 15 | 96/07/06/01:27:05.5 | 22.67 | 120.51 | 24 | -0.71 | 0.83 | -0.65 | -1.73 | 0.17 | 1.32 | 4.19 | 257 | 53 | -8 | 0.520 | 26.5 | C3 |
| 16 | 96/07/17/09:26:56.6 | 23.90 | 122.48 | 24 | -2.96 | 0.52 | 3.11 | 1.23 | 3.61 | -1.73 | 4.41 | 262 | 20 | 106 | 0.535 | 23.2 | C2 |
| 17 | 96/07/27/00:26:39.5 | 24.33 | 122.03 | 21 | 2.46 | -4.33 | 2.71 | -2.93 | 10.76 | -13.81 | 4.78 | 132 | 14 | 8 | 0.397 | 30.0 | B3 |
| 18 | 96/07/29/20:20:53.5 | 24.49 | 122.35 | 63 | 4.63 | -72.97 | 62.35 | 76.99 | 49.39 | 57.29 | 5.34 | 66 | 51 | 148 | 0.352 | 16.4 | B2 |
| 29 | 96/08/05/18:41:13.5 | 23.17 | 121.70 | 45 | 0.46 | -2.22 | 1.71 | 1.48 | -1.48 | -0.09 | 4.25 | 352 | 50 | 37 | 0.331 | 3.0 | B1 |
| 20 | 96/08/10/06:23:05.7 | 23.89 | 122.65 | 48 | -241.58 | 72.30 | 195.17 | 41.06 | 299.59 | -221.44 | 5.70 | 290 | 22 | 140 | 0.535 | 5.2 | C1 |
| 21 | 96/09/01/15:55:41.8 | 24.46 | 121.92 | 27 | 0.36 | -0.07 | -0.03 | -0.74 | 0.06 | -0.47 | 3.91 | 97 | 58 | -6 | 0.487 | 12.8 | B2 |
| 22 | 96/09/05/18:12:47.2 | 24.53 | 122.27 | 57 | -0.04 | -0.62 | 0.46 | 0.02 | 0.23 | 0.47 | 3.86 | 19 | 27 | 122 | 0.282 | 9.2 | A1 |
| 23 | 96/09/06/02:04:56.4 | 21.93 | 121.37 | 24 | 21.92 | -61.97 | 21.65 | 16.01 | 31.72 | 26.04 | 5.15 | 46 | 48 | 154 | 0.548 | 9.1 | C1 |
| 24 | 96/09/06/11:34:32.7 | 21.69 | 121.32 | 24 | -8.14 | -33.50 | 21.57 | -16.08 | 22.98 | -64.05 | 5.19 | 133 | 19 | 31 | 0.563 | 27.7 | C3 |
| 25 | 96/09/06/14:37:31.7 | 21.70 | 121.36 | 27 | -0.77 | 0.39 | 0.09 | -0.17 | 0.77 | -0.60 | 3.98 | 318 | 32 | 170 | 0.587 | 5.3 | C1 |

Table 2. continued.

| | | | | | | | | | | | | | | | | | |
|----|---------------------|-------|--------|----|-------|-------|-------|-------|-------|--------|------|-----|----|------|-------|------|----|
| 26 | 96/09/09/01:52:38.6 | 24.31 | 121.83 | 15 | -0.24 | -1.29 | 1.06 | -3.04 | -1.64 | 1.58 | 4.34 | 282 | 63 | 27 | 0.408 | 24.1 | B2 |
| 27 | 96/10/01/07:54:24.9 | 22.96 | 120.86 | 18 | 1.5 | 3.81 | -3.01 | 3.48 | -1.73 | -4.93 | 4.51 | 302 | 24 | -125 | 0.450 | 36.2 | B3 |
| 28 | 96/10/09/09:29:05.7 | 23.62 | 121.00 | 15 | 2.68 | -1.76 | -0.11 | 2.54 | -1.30 | -0.36 | 4.31 | 341 | 75 | 9 | 0.500 | 38.7 | B3 |
| 29 | 96/11/01/09:08:03.8 | 23.21 | 121.46 | 18 | -0.44 | -1.57 | 1.74 | 0.84 | -0.35 | 0.30 | 4.13 | 23 | 39 | 82 | 0.373 | 8.2 | B1 |
| 30 | 96/11/14/01:39:11.2 | 23.42 | 122.09 | 33 | 4.22 | -9.01 | 4.49 | 1.62 | -2.57 | 0.13 | 4.55 | 332 | 58 | 34 | 0.386 | 44.4 | B4 |
| 31 | 96/11/26/08:22:23.7 | 24.16 | 121.70 | 24 | 10.57 | -8.18 | 5.20 | -1.94 | 4.47 | -30.67 | 4.95 | 131 | 11 | 31 | 0.547 | 39.5 | C3 |
| 32 | 96/11/27/07:45:13.3 | 23.88 | 122.49 | 27 | -3.22 | 1.10 | 2.26 | -1.31 | 3.86 | -0.77 | 4.41 | 317 | 27 | 143 | 0.618 | 25.9 | C3 |
| 33 | 96/12/18/02:50:08.6 | 22.80 | 121.38 | 18 | -0.09 | -2.27 | 1.55 | 1.06 | -1.52 | 0.88 | 4.24 | 356 | 34 | 45 | 0.424 | 9.8 | B1 |
| 34 | 96/12/18/11:20:23.2 | 22.82 | 121.36 | 18 | -1.91 | -2.49 | 5.17 | 2.48 | -2.83 | -1.62 | 4.45 | 19 | 46 | 53 | 0.472 | 46.3 | B4 |
| 35 | 96/12/25/21:52:16.6 | 24.16 | 122.34 | 24 | -8.51 | 2.10 | 8.30 | 0.41 | 4.93 | -3.52 | 4.62 | 288 | 33 | 125 | 0.559 | 7.1 | C1 |
| 36 | 96/12/28/21:08:06.5 | 24.00 | 122.46 | 42 | -8.96 | 4.28 | 3.88 | -3.85 | 15.20 | -6.51 | 4.78 | 323 | 24 | 162 | 0.627 | 4.5 | C1 |

¹ Origin time (O.T.: Year/Month/Day/hr:min:sec) and epicentral locations (°N, °E) are reported by the Seismological Observation Center, Central Weather Bureau, Taiwan.

² X, Y, Z point to north, east, and vertically down, respectively. All are in the unit of 1×10^{15} Nt m.

³ Estimated best double-couple solutions in degrees.

⁴ E and ϵ are defined by equations (4) and (2).

The inland event (No. 6) shows a thrust mechanism with a slightly oblique component (Figure 7). Based on the NW–SE oriented *P*-axis, this event probably shares the same tectonic origin as that of event No. 29. The distribution of misfit indicates a well-defined minimum at 15 ± 3 km and most of the available *P* wave first-motion polarities are compatible with our solution.

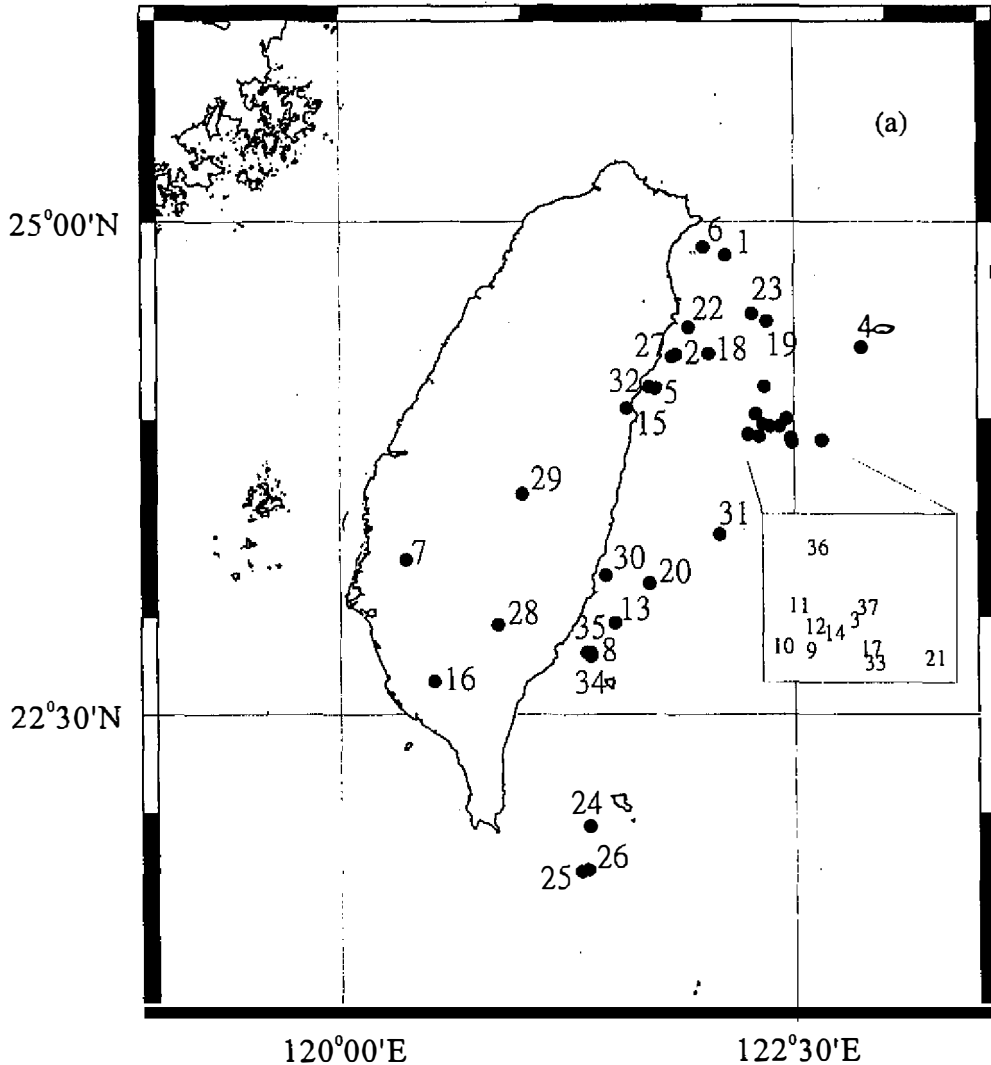
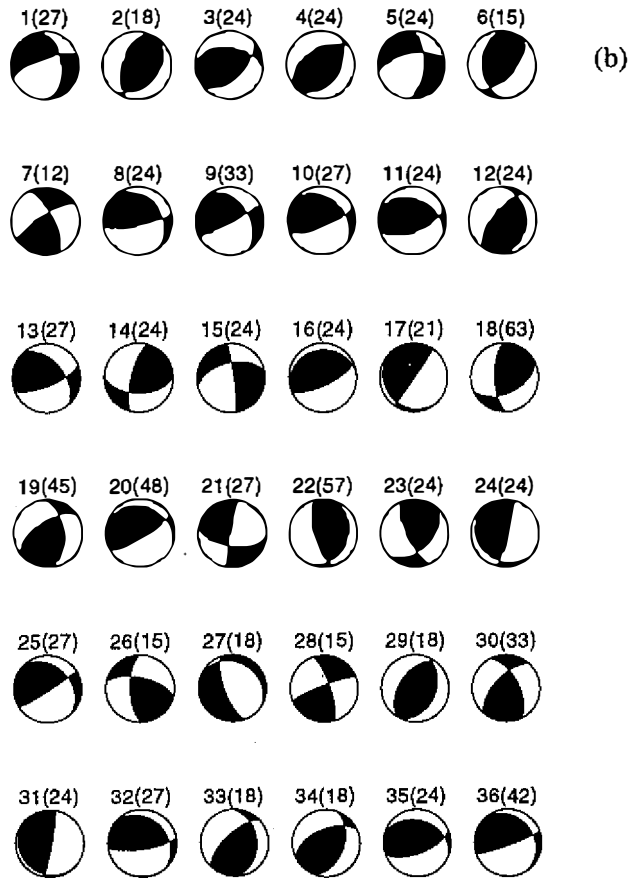


Fig. 4. Moment –tensor inversion results. (a) Map shows the epicenters of 36 earthquakes presented in this study. Numbers are according to Table 2. (b) Corresponding best double-couple solutions. The first number above each fault plane solution is the event number. The number in parenthesis is the best focal depth.



(Fig. 4. continued)

4. DISCUSSION

Of the earthquakes reported here, CMT solutions for 5 large and moderate-sized events were also announced by other institutions (Harvard University and/or the USGS). To check the consistency among them, we list these various results in Table 3. The similarity between two fault plane solutions is represented as

$$\psi = 1 - [(\delta\theta_p + \delta\theta_t) / 180^\circ] \quad (5)$$

where $\delta\theta_p$ is the angle between the two solutions' P -axes, and $\delta\theta_t$ is that between the T -axes. If two fault plane solutions are exactly the same, the parameter ψ is 1, whereas if the two show exactly the opposite sense of deformation (e.g., pure thrust vs. pure normal faulting on the same plane), ψ would be 0.

In general, we regard our solutions to be quite similar to other reported CMT solutions with most having $\psi \geq 0.75$ (Table 3), that translates into an average angle difference of $\sim 20^\circ$

for P - T -axes. One exception is event No. 24 (September 6, 1996, 11:34:32.7; Tables 2 and 3 and Figure 4). Our solution shows a low-angle thrust focal mechanism with one nodal plane dipping shallowly westward, whereas the CMT solution from Harvard indicates an oblique thrust with both nodal planes at high angles (Table 3). In addition, our best solution gives the depth at 24 km, significantly deeper than the 15 km given by the Harvard CMT solution. The magnitude of this event is barely enough for body waveform inversion using teleseismic records (e.g., Nabelek, 1984; Kikuchi and Fukao, 1987) and we have failed to obtain a satisfactory solution this way. Therefore, it is difficult to determine which solution describes the source more correctly at this moment and, subsequently, what causes the discrepancy. Nevertheless, both solutions give consistent patterns of thrust mechanism and nearly E-W oriented P -axes that would not conflict with the known tectonic setting in that particular region (e.g., Kao et al., 1999).

We have done a thorough control study on the reliability of our inversion results. A detailed discussion of our control study is beyond the scope of this paper and will be addressed by a separate report (Kao and Jian, manuscript in preparation, 1999). Based on our experiences, the most influential factors are (1) the complexity of velocity structures along source-station paths, (2) the degree of mislocation of epicenters, and (3) the number of stations used in the inversion and their azimuthal distribution.

There are two ways to minimize the misfit resulting from complex structures. One is to include a more detailed velocity model in calculating the Green's functions; another is to use only the long-period waveforms in the inversion (e.g., Ritsema and Lay, 1995). Our two-step inversion procedure is a combination of both approaches. We design the first step to select the best "simplified" velocity model for each station, whereas the inversion utilizes the long-period waveforms to ignore the velocity details. The drawback, however, is that the inversion is inapplicable to small earthquakes because they usually fail to generate sufficient long-period energy. At the moment, we set the threshold at $M_L \geq 4.5$.

For the majority of earthquakes that we have studied, the best solutions obtained by our two-step inversion procedure are very similar, if not identical, to those inverted with a fixed velocity model, yet give smaller misfit between observed and synthetic waveforms. In other words, the main effect of choosing different velocity models for different stations is to improve the waveform correlation rather than to alter the solution (i.e., the misfit caused by the velocity model can be reasonably separated from that by the source). This is not surprising because at the frequency band adapted in our inversion, details of the velocity model are relatively insignificant compared to source properties. Nevertheless, it is always desirable to prescribe a more realistic (and correct) velocity model in calculating the Green's functions. As soon as we have sufficient *a priori* knowledge of the velocity details, the inversion can be further applied to smaller events using a higher frequency band.

Similarly, erroneous results may be caused by epicentral mislocation in both azimuth and distance. Our control study indicates that, despite using only the long-period waveforms in the inversion, a mislocation of ≥ 15 km in distance or $\geq 10^\circ$ in azimuth would result in a 15° deviation from the true solution (particularly for the strike of a strike-slip fault), if a single-station inversion is performed. Inclusion of data from another station may significantly improve the mislocation tolerance if the azimuthal gap is $\sim 90^\circ$. Generally speaking, reliable

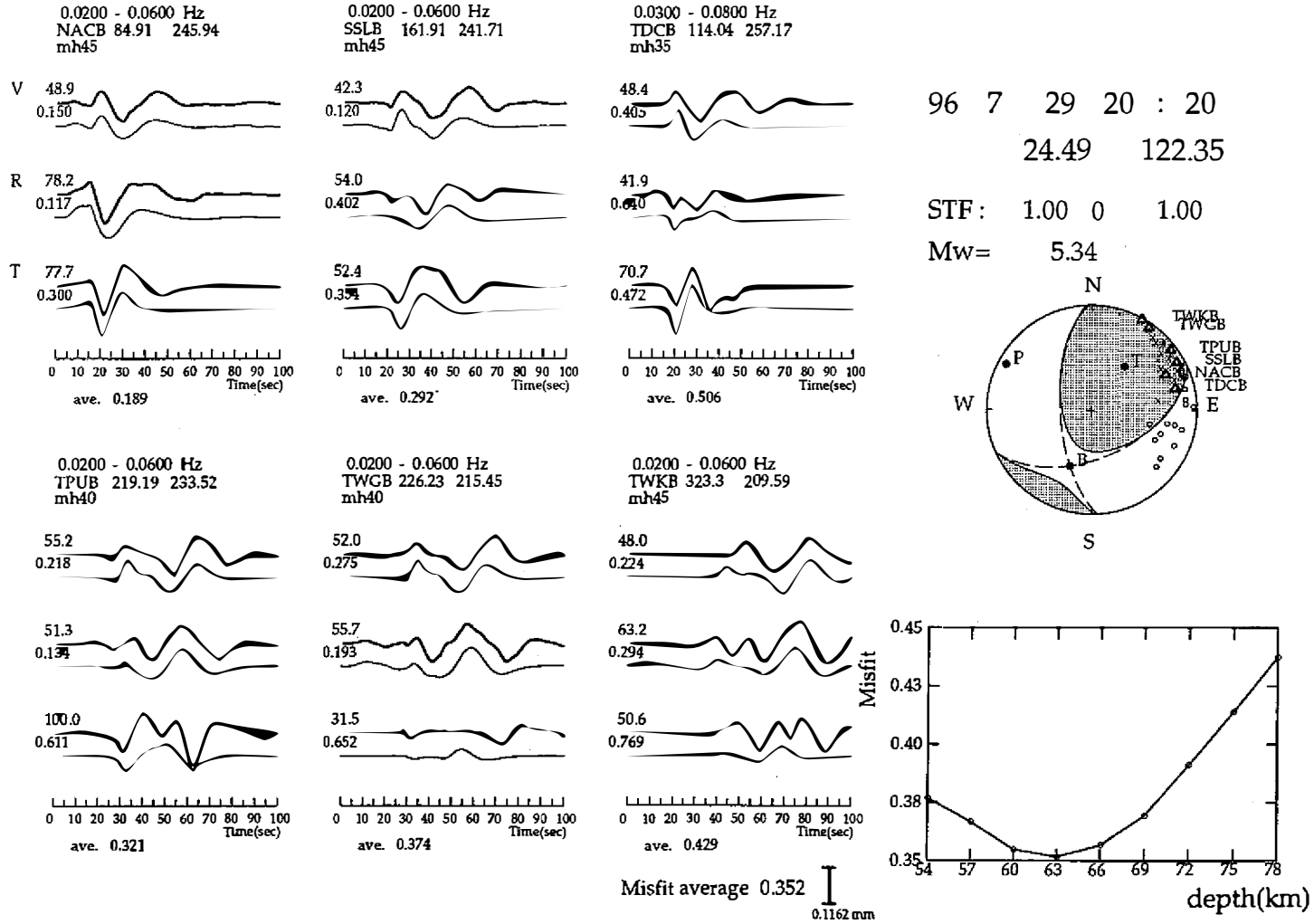


(Fig. 5. Caption is on the next page)

Fig. 5. Moment-tensor inversion of event No. 18 (July 29, 1996). Seismograms of three components (V: vertical; R: radial; T: transverse) from six BATS stations are used. The station code, azimuth, epicentral distance, name of velocity model, and the frequency band used in the inversion are shown at the top of each set of seismograms. Thick and thin traces are observed and synthetic waveforms, respectively. The normalized maximum amplitude and corresponding misfit are near the beginning of each trace. The absolute amplitude scale is shown near the bottom. The focal mechanism is shown in lower-hemisphere projection with shaded area showing compressional *P* first motions. Dashed lines represent the corresponding best double couple solution. Solid dots mark the *P*, *T*, and *B* axes, while the open triangles show projected locations of used BATS stations. Open circles and crosses indicate dilatational and compressional *P* first motions, respectively, as reported by the local short-period stations. The plot of misfit versus focal depth indicates the best fit at 63 km, although there seems to be no significant difference among solutions from 60 to 66 km. The source time function (STF) is assumed to be a simple triangle of 2 s.

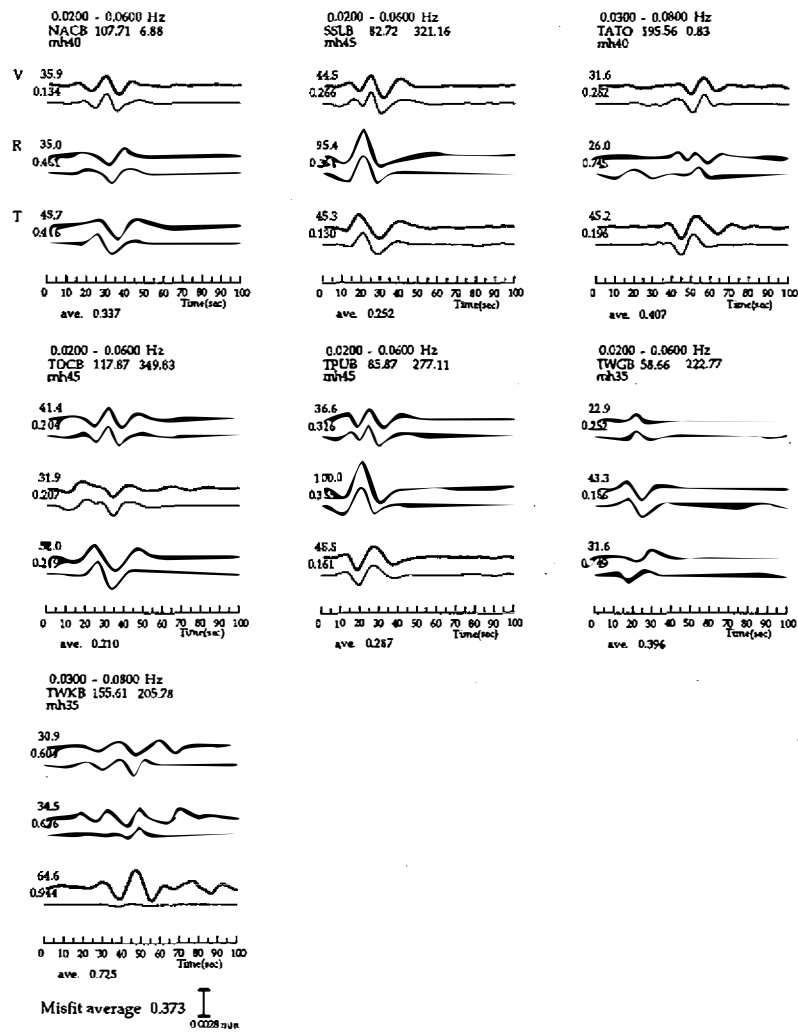
solutions can be obtained from a combined data set of three stations that covers at least two quadrants of the focal sphere.

5. CONCLUSION

By taking advantage of the BATS data, we are able to systematically determine source parameters for regional earthquakes in Taiwan. The choice of a different frequency band and velocity model depends on each station's background noise level and structural setting, respectively, making the inversion less sensitive to the island's high background noise and complex velocity heterogeneity. We evaluate the quality of our inversion by the misfit between the observed and synthetic waveforms (classified into A–F, Table 1) and the amount of the CLVD component (classified into 1–4, Table 1). In total, solutions for 36 events are reported in this study and all of them have an inversion quality higher than C4.

Three representative examples of inversion are shown in this paper to demonstrate the advantage of our technique. For the event that occurred at intermediate depth off NE Taiwan, our solution shows the *P*-/*T*-axis oriented parallel to the downdip direction of the subducted slab and the strike of the trench axis, respectively. This pattern is consistent with the downdip extension and lateral compression strain regimes inferred by previous studies (e.g., Kao and Chen, 1991; Kao et al., 1998b). An offshore event to the east of Taiwan and another inland earthquake in SW Taiwan both show thrust mechanisms with *P*-axes in a NW–SE direction, which is compatible with the interpretation that they manifest the effects of regional collision.

Most of our solutions are compatible with available *P* wave first motions recorded by the local short-period network and/or CMT solutions reported by other institutions. We intend to



96 11 1 9 : 8
 23.21 121.46
 STF: 1.00 0 1.00
 Mw= 4.13

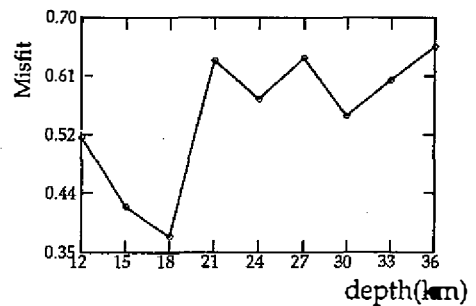
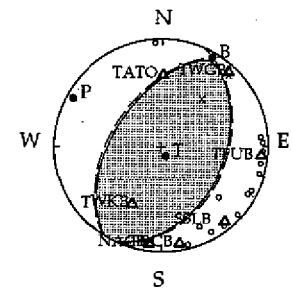
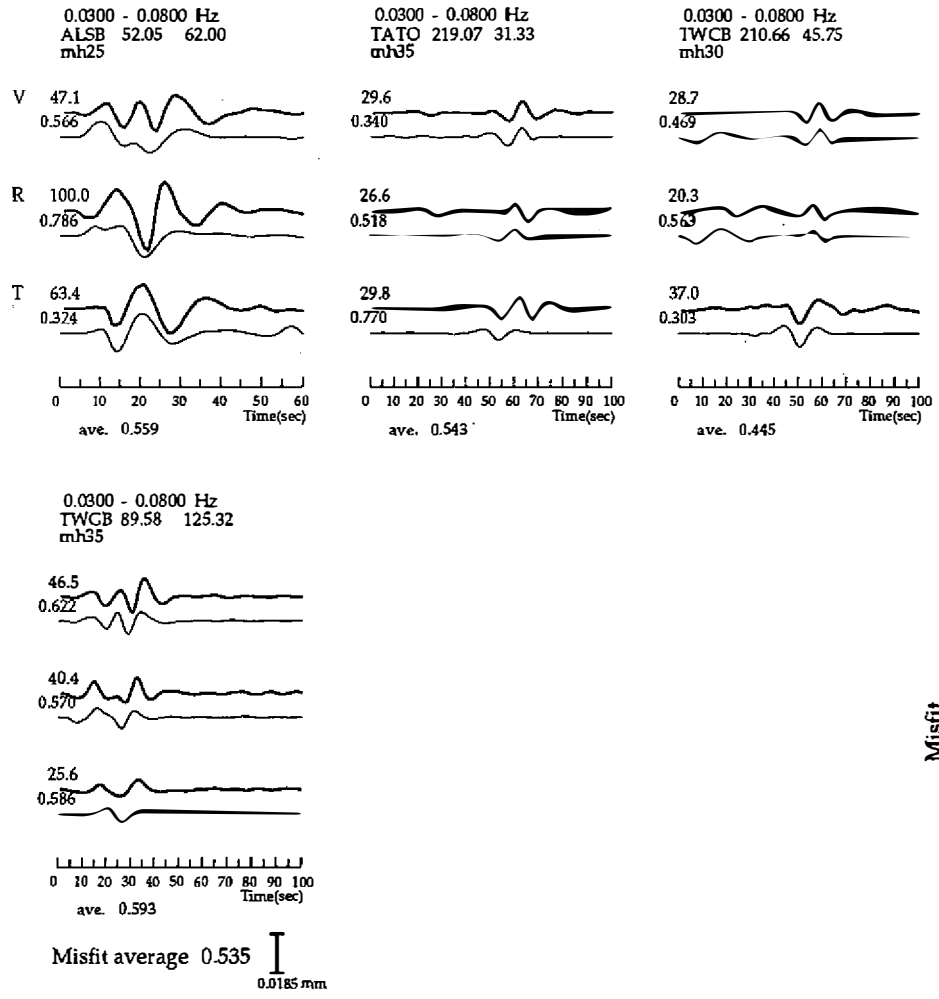


Fig. 6. Moment-tensor inversion of event No. 29 (November 1, 1996). Seismograms from seven BATS stations are used in the inversion. Layout is the same as in Figure 5.



95 10 31 22 : 27
23.29 120.36

STF: 1.00 0 1.00
Mw= 4.50

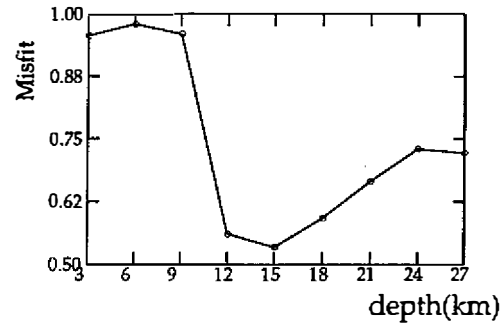
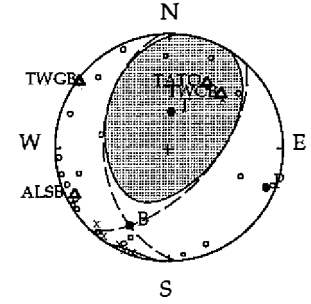


Fig. 7. Moment-tensor inversion of event No. 6 (October 31, 1995). Seismograms from four BATS stations are used in the inversion. Notice that station ALSB was a temporary station and is not shown in Figure 1. Layout is the same as in Figure 5.

Table 3. Comparison of BATS solutions and CMT solutions from other institutions.

| Event No. | CMT solutions | | | | | | BATS solutions | | | | | ψ^2 |
|-----------|---------------|-----|------|-------|-------|--------------------|----------------|-----|------|-------|-------|----------|
| | Strike | Dip | Rake | M_w | Depth | Inst. ¹ | Strike | Dip | Rake | M_w | Depth | |
| 11 | 302 | 17 | 145 | 5.7 | 21 | HV | 292 | 37 | 126 | 5.6 | 24 | 0.78 |
| 11 | 277 | 12 | 133 | 5.7 | 21 | USGS | 292 | 37 | 126 | 5.6 | 24 | 0.73 |
| 18 | 176 | 51 | 46 | 5.4 | 68 | HV | 66 | 51 | 148 | 5.3 | 63 | 0.85 |
| 20 | 286 | 29 | 151 | 5.6 | 33 | HV | 290 | 22 | 140 | 5.7 | 48 | 0.87 |
| 24 | 5 | 38 | 120 | 5.4 | 15 | HV | 133 | 19 | 31 | 5.2 | 24 | 0.54 |
| 31 | 138 | 1 | 20 | 5.2 | 15 | HV | 131 | 11 | 31 | 5.0 | 24 | 0.85 |

¹ HV: Harvard University; USGS: United States Geological Survey.

² ψ is defined by equation (5).

make our inversion results available on a routine basis that can not only provide precise source parameters for smaller regional earthquakes, but also serve as an alternative to independently examine solutions of large and moderate-sized events from other sources.

Acknowledgments The technical staff at IES led by Chun-Chi Liu assume primary responsibility for maintaining BATS. Data processing and archiving were performed by Jung Yang, Rong-Yu Chen, and Yu-Hwa Liu. We benefited from a short course offered by IRIS and instructed by Doug Dreger and Chuck Langston in December 1995. Part of the inversion code was originally written by Bor-Shouh Huang. Constructive discussions with Bao-Hen Chin, Wang-Ping Chen, Doug Dreger, Bor-Shouh Huang, Thorne Lay, Kuo-Fong Ma, Chen-Ying Wang, and Francis T. Wu are greatly appreciated. Comments from two anonymous reviewers have significantly improved an earlier version of the manuscript. This research was partially supported by the National Science Council, Republic of China, under grants NSC85-2111-M-001-020-Y and NSC86-2116-M-001-005-Y.

APPENDIX Figures in this Appendix, numbered according to their order of appearance in Table 2, show the complete result of waveform inversion. The layout is the same as in Figure 5. Interested readers can download an electronic version (in PostScript format) from the anonymous ftp server of the Institute of Earth Sciences, Academia Sinica (140.109.80.2). Hard copies are also available directly from the authors.

REFERENCES

- Aki, K., and P. G. Richards, 1980: Quantitative seismology: Theory and methods, 932 pp., Freeman, San Francisco.
- Bouchon, M., 1981: A simple method to calculate Green's functions for elastic layered media. *Bull. Seismol. Soc. Am.*, **71**, 959-971.
- Dreger, D. S., and D. V. Helmberger, 1993: Determination of source parameters at regional

- distances with three-component sparse network data. *J. Geophys. Res.*, **98**, 8107–8125.
- Dziewonski, A. M., T.-A. Chou, and J. H. Woodhouse, 1981: Determination of earthquake source parameters from waveform data for studies of global and regional seismicity. *J. Geophys. Res.*, **86**, 2825–2852.
- Fan, G., and T. Wallace, 1995: Focal mechanism of a recent event in South Africa: A study using a sparse very broadband network. *Seismol. Res. Lett.*, **66**, 13–18.
- Kao, H., and W.-P. Chen, 1991: Earthquakes along the Ryukyu–Kyushu arc: Strain segmentation, lateral compression, and the thermomechanical state of the plate interface. *J. Geophys. Res.*, **96**, 21,443–21,485.
- Kao, H., P.-R. Jian, K.-F. Ma, B.-S. Huang, and C.-C. Liu, 1998a: Moment-tensor inversion for offshore earthquakes east of Taiwan and their implications to regional collision. *Geophys. Res. Lett.*, **25**, 3619–3622.
- Kao, H., S. J. Shen, and K.-F. Ma, 1998b: Transition from oblique subduction to collision: Earthquakes in the southernmost Ryukyu arc–Taiwan region. *J. Geophys. Res.*, **103**, 7211–7229.
- Kao, H., G.-C. Huang, C.-S. Liu, 1999: Transition from oblique subduction to collision in the northern Luzon arc–Taiwan region: Constraints from bathymetry and seismic observations. *J. Geophys. Res.*, in press.
- Kawakatsu, H., 1995: Automated near-real-time CMT inversion. *Geophys. Res. Lett.*, **22**, 2569–2572.
- Kennett, B. L. N., 1980: Seismic waves in a stratified half space — II. Theoretical seismograms. *Geophys. J. R. Astron. Soc.*, **61**, 1–10.
- Kikuchi, M., and Y. Fukao, 1987: Inversion of long-period P-waves from great earthquakes along subduction zones. *Tectonophysics*, **144**, 231–247.
- Langston, C. A., 1981: Source inversion of seismic waveforms: the Koyna, India, earthquakes of 13 September 1967. *Bull. Seismol. Soc. Am.*, **71**, 1–24.
- Lay, T., J. Ritsema, C. J. Ammon, and T. Wallace, 1994: Rapid source-mechanism analysis of the April 29, 1993 Cataract Creek ($M_w = 5.3$), northern Arizona earthquake. *Bull. Seismol. Soc. Am.*, **84**, 451–457.
- Mellman, G. R., L. J. Burdick, and D. V. Helmberger, 1975: Determination of source parameters from body wave seismograms. *Earthquake Note*, **40**, 44.
- Nebelek, J. L., 1984: Determination of earthquake source parameters from inversion of body waves, Ph.D. thesis, Mass. Inst. of Technol., Cambridge.
- Pasyanos, M. E., D. S. Dreger, and B. Romanowicz, 1996: Toward real-time estimation of regional moment tensors. *Bull. Seismol. Soc. Am.*, **86**, 1255–1269.
- Rau, R.-J., and F. T. Wu, 1995: Tomographic imaging of lithospheric structures under Taiwan. *Earth Planet. Sci. Lett.*, **133**, 517–532.
- Ritsema, J., and T. Lay, 1995: Long-period regional wave moment tensor inversion for earthquakes in the western United States. *J. Geophys. Res.*, **100**, 9853–9864.
- Sipkin, S. A., 1982: Estimation of earthquake source parameters by the inversion of waveform data: synthetic waveforms. *Phys. Earth Planet. Inter.*, **30**, 242–259.
- Thio, H. K., and H. Kanamori, 1995: Moment-tensor inversions for local earthquakes using

- surface waves recorded at TERRAScope. *Bull. Seismol. Soc. Am.*, **85**, 1021–1038.
- Wallace, T. C., D. V. Helmberger, and G. R. Mellman, 1981: A technique for the inversion of regional data in source parameter studies. *J. Geophys. Res.*, **86**, 1679–1685.
- Yao, Z. X., and D. G. Harkrider, 1983: A generalized reflection-transmission coefficient matrix and discrete wavenumber method for synthetic seismograms. *Bull. Seismol. Soc. Am.*, **73**, 1685–1699.
- Zeng, Y., and J. G. Anderson, 1996: A composite source model of the 1994 Northridge earthquake. *Bull. Seismol. Soc. Am.*, **86**, S71–S83.
- Zhao, L.-S., and D. V. Helmberger, 1994: Source estimation from broadband regional seismograms. *Bull. Seismol. Soc. Am.*, **84**, 91–104.
- Zhu, L., and D. V. Helmberger, 1996: Advancement in source estimation techniques using broadband regional seismograms. *Bull. Seismol. Soc. Am.*, **86**, 1634–1641.